Int. J. Electrochem. Sci., 14 **(2019)** 9391 – 9403, doi: 10.20964/2019.10.13

International Journal of
ELECTROCHEMICAL
SCIENCE
www.electrochemsci.org

Nitrogen-doped Graphene Electrochemical Sensor for Selenium (IV) in Water

Colani T Fakude[1], *Omotayo A Arotiba*[1,2], *Richard Moutloali*[1,3], *Nonhlangabezo Mabuba*[1,2,*]

[1] Department of Chemical Sciences (prior known as Department of Applied Chemistry), University of Johannesburg, Doornfontein 2028, Johannesburg, South Africa,
[2] Centre for Nanomaterials Science Research, University of Johannesburg, South Africa
[3] Nanotechnology Innovation Centre DST/MINTEK, University of Johannesburg, South Africa
[*]E-mail: nmabuba@uj.ac.za

Received: 3 June 2019/ *Accepted:* 2 July 2019 / *Published:* 30 August 2019

In this study, the electrochemical detection of Se(IV) on a glassy carbon electrode (GCE) modified with nitrogen-doped graphene (NG) is reported. NG was synthesized from graphene oxide (GO) by thermal annealing of GO in ammonia. Structural and morphological studies of the synthesized NG were conducted using field emission scanning electron microscopy (FESEM), Raman spectroscopy, high resolution-transmission electron microscopy (HR-TEM), Fourier Transform -infrared spectroscopy (FT-IR) and a CHNS analyzer. Electrochemical characterization of the unmodified GCE and the NG modified GCE (GCE-NG) was conducted using cyclic voltammetry (CV) and electrochemical impedance spectroscopy (EIS). The newly developed GCE-NG sensor demonstrated improved electrochemical properties when compared to the bare GCE. Square wave anodic stripping voltammetry (SWASV) was employed to optimize the proposed sensors' detection parameters: 0.1 M $HClO_4$ supporting electrolyte, -0.8 V deposition potential and 50 s deposition. The calibration graph of Se(IV) concentrations and current response demonstrated linearity during the calibration of the sensor in the concentration range 1 – 120 ppb, with a limit of detection (LOD) of 0.092 ppb. The proposed electrochemical sensor was applied in the analysis of real water samples and inductively coupled plasma-optical emission spectroscopy (ICP-OES) was used to validate the results.

Keywords: Electrochemical sensor; selenium; nitrogen-doped graphene; square wave anodic stripping voltammetry

1. INTRODUCTION

Selenium (Se) is a micro-nutrient which plays a significant role in the growth and health of both humans and animals. However, in recent years, this trace element has gained attention from researchers due to the health risks it poses to humans when found in high levels in dams, rivers, and groundwater or when the intake dosage surpasses the recommended 400 µg per day [1].For this reason, the World Health

Organization and other water quality control organizations have set numerical limits of 10 ppb for Se in drinking water [2,3,4].

Selenium is found in the environment in several oxidation states, VI, IV, 0 and –II. Se(IV) is considered as the most toxic and the only electroactive form of selenium [1]. The problems associated with selenium make it necessary to control and monitor Se(IV) amounts in drinking water by means of sensitive techniques. There are several routine techniques that have been reported for Se analysis, including atomic absorption spectrophotometry (AAS) [4], high-performance liquid chromatography (HPLC) [3], and gas chromatography (GC) [5]**.** Unfortunately, these methods are costly, laboratory borne, time-consuming, and may need highly trained personnel to operate them [6]. Electroanalytical techniques, especially anodic stripping voltammetry (ASV), have been reported to be better alternatives to the conventional methods because they do not only offer high sensitivity but are also user-friendly, portable, use less power and take less time for sample preparation and analysis [5,7]. Electrochemical sensing method by using ASV is also amenable to improvement and one of the ways of achieving this is by the use of electrode modifiers.

Nanomaterials such as gold nanoparticles, carbon nanotubes, and graphene,etc. have been reported as modifiers for sensing of Se (IV) in water samples. For example, a limit of detection (LOD) of 0.22 ppb for Se(IV) was reported by Arotiba and co-workers when gold nanoparticles were used as a modifier on a glassy carbon electrode [8]. The same team of researchers also reported the use of reduced graphene oxide as an electrode modifier for selenium detection and a LOD of 0.85 ppb was obtained [9]. Sadie and co-workers achieved a LOD of 0.42 ppb when using a micro-fabricated gold ultra-microelectrode array to detect selenium using square wave anodic stripping voltammetry [5].

Graphene has attracted tremendous attention for its distinct thermal, mechanical, optical, electronic properties and high surface area, thereby rendering it a modifier of interest in electrochemistry [10]. Its sp^2-bonded atoms are the reason for its excellent chemical and electronic properties leading to the development of electron transfers in redox systems. For this reason and also owing to its low cost, graphene has been used to develop simple and improved electrochemical sensors [11].

Recent reports have shown that electronic traits of graphene can be tailored by chemical doping with hetero-atoms such as N, B, S, and P [12]. Nitrogen can be regarded as suitable atom for doping because it has a similar atomic size as carbon and one extra electron in its valence shell [13]. Therefore, doping with nitrogen enriches charge carrier densities and enhances electrical and thermal conductivities of graphene due to the contribution of 2 electrons to the π-system. Thus, N-doped graphene has gained considerable attention for fuel cells applications [14], biosensors [15] and sensor electrode modification [13].

This article reports for the first time, the use of nitrogen-doped graphene (NG) as an electrode modifier for the detection of Se(IV) in drinking water samples.

2. EXPERIMENTAL

2.1 Materials and Instruments

The chemicals used in this study were of analytical grade and were used as received. They were purchased from Sigma Aldrich (South Africa). The chemicals include selenium standard for ICP, cadmium standard for ICP, Magnesium sulfate, cupric nitrate, sulfuric acid (98%), sodium nitrate, hydrogen peroxide (30%), disodium hydrogen phosphate, potassium ferricyanide, potassium ferrocyanide, sodium dihydrogen phosphate, potassium permanganate, nitric acid, potassium chloride, natural graphite, ammonium hydroxide (30%), hydrochloric acid (30%), hydrazine monohydrate, sodium hydroxide, N-N dimethylformamide (DMF), hydrochloric acid (5%), potassium hydroxide, hydrogen peroxide (30%) and ethylenediaminetetra-acetic acid (EDTA). Deionized water was used for the preparation of standards. The real sample analysed in this study was obtained from the electrochemistry laboratory and it was analyzed within the same day of sampling.

The micrographs of the materials were obtained using a field emission scanning electron microscope (FESEM) on a JOEL JSM FESEM 7500F (Japan) instrument and high-resolution transmission electron microscope (HR-TEM) on a JEOL 2100 HRTEM 200V (Japan).

X'Pert Pro Panalytical X-ray Diffractometer was employed for X-ray diffraction measurements (Rigaku Ultima IV, Japan) bearing Cu-K_α radiation (λ= 0.15406 nm) and scanning angle (2θ) ranging from 4^0 to 80^0. Fourier Transmission Infrared (FT-IR) spectra were obtained using Bruker-Alpha FTIR (South Africa), following the traditional KBr compression method. Elemental analysis was investigated using the Thermofisher Scientific Flash 2000 Organic Elemental Analyzer (USA).

An Ivium Compactstat potentiostat (Netherlands) system connected to a three-electrode system was used to conduct all electrochemical measurements. The electrode system comprised of a counter electrode (platinum wire), a working electrode (3 mm diameter bare and modified glassy carbon electrode) and a reference electrode (Ag/AgCl in 3M KCl). All the electrochemical measurements were conducted against the Ag/AgCl reference electrode. Before conducting the electrochemical experiments, the electrochemical cells were purged with ultra-pure argon gas for 4-5 minutes.

2.2 Synthesis of Graphene Oxide and Nitrogen-doped Graphene

Graphite powder was used for the preparation of graphene oxide (GO) following the modified Hummers' method [16]. NG was prepared by the thermal annealing of GO in ammonia. This has been reported to produce monolayer graphene films and reduced the interlayer distance by removing impurities and oxygen-containing functional groups [17]. Briefly, 140 mg of GO was dispersed in water by ultrasonic agitation followed by the addition of $NH_3 \cdot H_2O$ (30%) to attain pH 10. The mixed suspension was stirred for 10 min, after which 2 mL of hydrazine was added. The solution was incubated in the oven at 80 °C for 12 h to allow the reduction of the graphene oxide by hydrazine, which was seen by the production of a black precipitate. The precipitate was washed three times with double distilled water and its pH was adjusted to neutral. Eventually, NG was obtained after drying the solid product in the last step [18].

2.3 Electrode fabrication

Alumina slurries of different sizes (1, 0.3 and 0.05 µm) were used to mechanically polish the bare GCE using a polishing pad. The electrode was ultrasonicated in ethanol and water to remove any physically adsorbed substances. Subsequently, 10 mg of NG was dispersed in 10 ml of DMF by sonicating for an hour. The modification of the electrode was carried out by drop coating 8 µl of the colloidal suspension on to the electrode surface and allowed to dry in the air, at room temperature. The modified electrode was reported as GCE-NG.

2.4 Electrochemical characterization of bare GCE and GCE-NG

The electrochemical behavior of the unmodified GCE and GCE-NG was investigated in a neutral solution containing 5 mM $[Fe(CN)_6]^{3-/4-}$(1:1) as a redox probe with a supporting electrolyte of 0.1 M KCl. Cyclic voltammetry (CV) and electrochemical impedance spectroscopy (EIS) were conducted to characterize the electrode. For the CV measurements, the potential window was -0.4 to 0.8 V at 50 mV/s scan rate. For the EIS analysis, a bias potential of 0.22V was used at 100 KHz to 100 mHz frequency range as well as at 5 mV alternate potential. Square wave anodic stripping voltammetry (SWASV) was applied for the quantitative detection of Se(IV) using the following settings: pulse amplitude at 50 mV and SWASV frequency of 25 Hz.

3. RESULTS AND DISCUSSION

3.1 Structural and morphological characterization

3.1.1 FESEM and HRTEM analysis

FESEM and HRTEM were employed to characterize the surface morphology and crystalline structures of the prepared NG. The FESEM image of NG, presented in **Fig. 1(a**), showed sheets of carbon layers as expected. This was verified by the thin films observed with HRTEM **(Fig. 1(b)).**

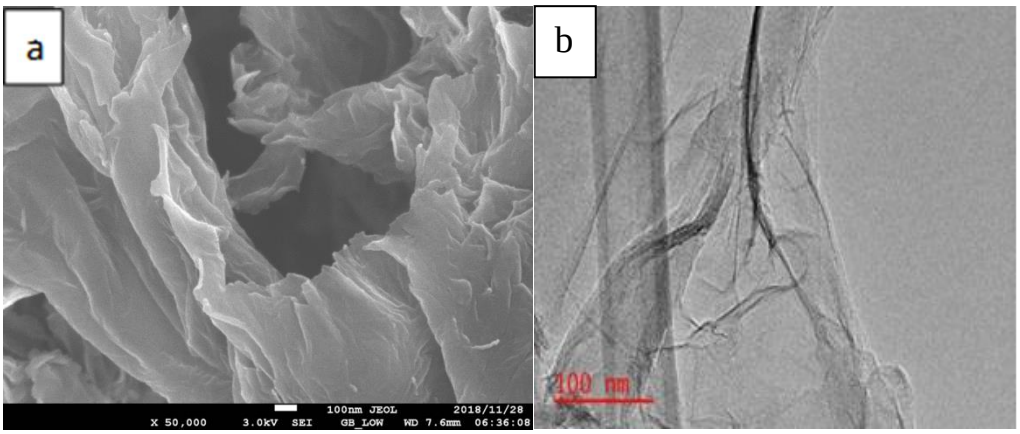

Figure 1. (a) FESEM image and **(b)** HRTEM image of NG.

3.1.2 XRD analysis

XRD analysis was conducted to investigate the crystalline changes that occurred during the synthesis of GO and NG and to determine the d-spacing variations in the layers of the materials. For GO (**Fig. 2**), a sharp peak is observed at 2θ= 11.5°, thereby indicating the oxidation of graphite to GO. Bragg's law was used (**Eqn. 1**) [19], where the wavelength was represented by lambda (λ = 0.15406 nm), peak position (2θ = 11.5) and the interlayer spacing (d) was determined to be 7.6885 Å**.**

$(n\lambda = 2d\sin\theta)$ **Equation (1)**

After the reduction process, which eliminated most of the intercalated oxygen-containing functional groups, NG showed a broader peak at 2θ = 24.5° with a d-spacing of 3.6305 Å, indicating the restoration of the π-conjugated structure of graphene [14]. The reduction of the d-spacing from 7.6885 Å to 3.6305 Å proved that the oxygen moieties were efficiently removed, resulting in closely packed NG sheets [20].

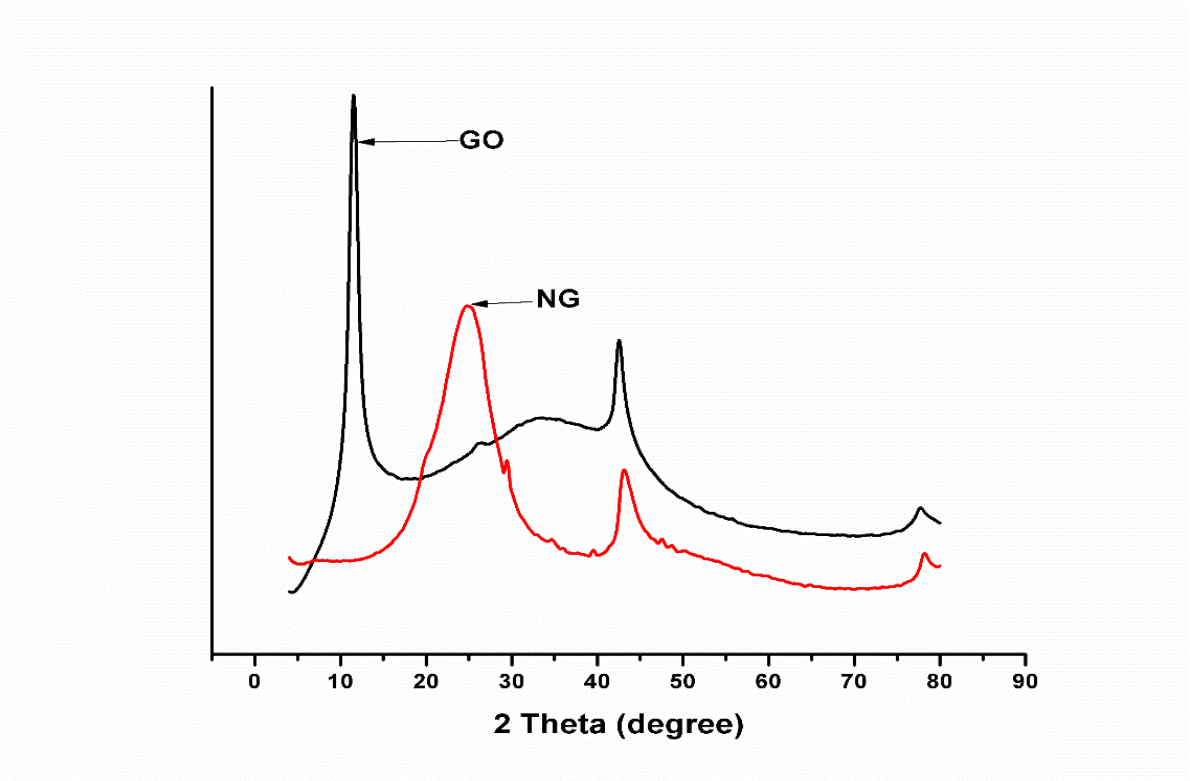

Figure 2. XRD spectra of GO and NG

3.1.3 FT-IR analysis of GO and NG

FT-IR analysis was conducted to identify the different functional groups present in the prepared GO and NG samples. As displayed in **Fig. 3**, the spectra of GO exhibited many oxygen functional groups in its structure. The peaks at 3438, 2358, 1624, 1402, 1247, 1191and 1042 cm^{-1}were ascribed to the stretching vibrations of hydroxyl (OH), carbon dioxide (CO_2), aromatic skeleton carbon ring (C=C), carboxyl (C-O), epoxyl (O-C-O), aldehyde (C-OH) and alkoxyl (C-O), respectively. Those at 2933 and

2848 cm^{-1} were ascribed to C-H groups [21]. The spectra of NG displayed decreased intensities of the oxygen-containing functional groups. For example, the peak for CO_2 (2358 cm^{-1}) disappeared almost completely in NG, indicating the escape of CO_2 gas from the lattice during the hydrazine-induced reduction process. The peaks at 1624 cm^{-1} and 1191 cm^{-1} could be due to the presence of N heteroatoms in the lattice structure, and hence can be attributed to the stretching vibrations of C=N and C-N bonds (sometimes C=C and C=N bonds can stretch at the same wavelength) [12,21]**.** The decreased intensities of the stretching vibrations of the oxygen moieties also suggested effective reduction.

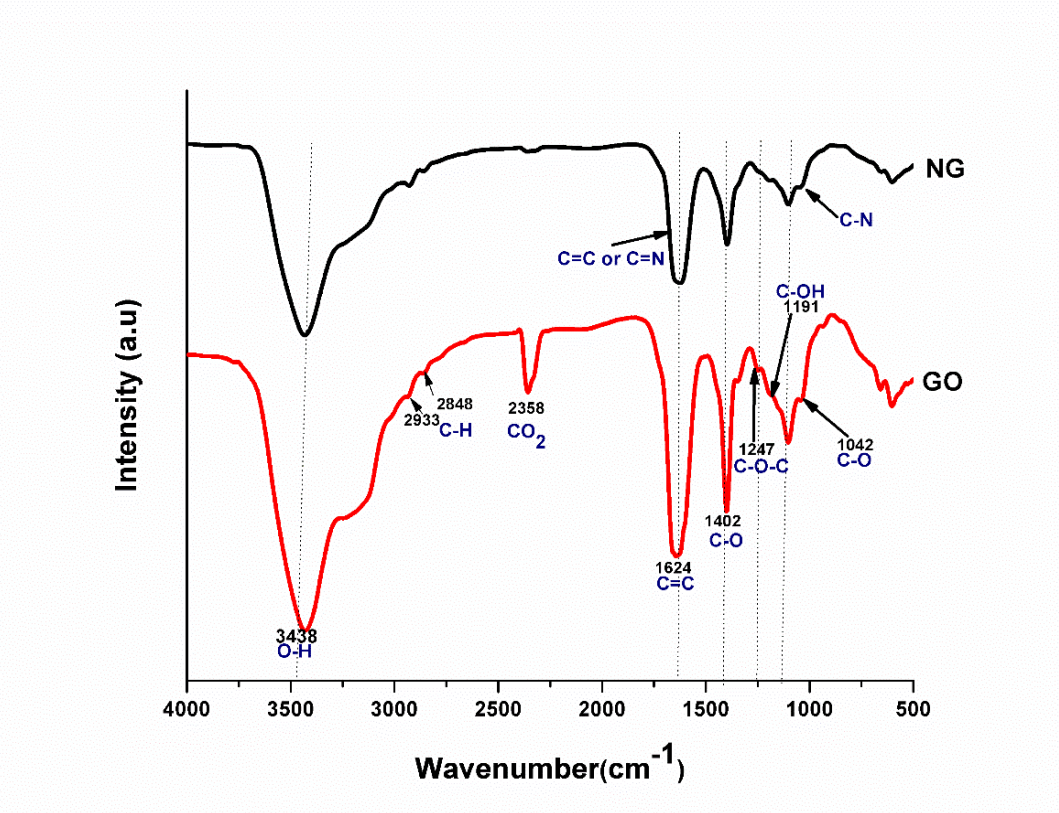

Figure 3. FTIR spectra of GO (red) and (black).

3.1.4 Elemental analysis

CHNS elemental analysis was conducted to determine the chemical compositions of the prepared GO and NG samples so as to confirm the introduction of nitrogen into the graphene lattice. The percentage weight composition of each sample is presented in **Table 1**. The amount of oxygen (20.8%) was determined from the difference between the sum of C (73.29%), H (1.11%) and N (4.8%), based on the assumption that ash was not present. In the NG sample, the oxygen content was low compared to GO which confirmed successful reduction and the N content in NG verified the introduction of N (4.8%) into the graphene lattice.

Table 1. Composition of different atoms in GO and NG by percentage weight.

SAMPLE	N%	C%	H%	O%
GO	0	47.89	1.84	50.27
NG	4.8	73.29	1.11	20.8

3.2. Electrode characterization

The unmodified GCE and GCE-NG electrodes were characterized by CV and well defined anodic and cathodic peaks appeared as indicated in **Fig. 4a**. The modified electrode displayed a significantly higher anodic peak current (93 µA) when compared to the unmodified GCE (60 µA). This was due to the enhanced electron conducting properties of NG in facilitating electron transfer between the GCE surface and ferri/ferrocyanide solution [13].

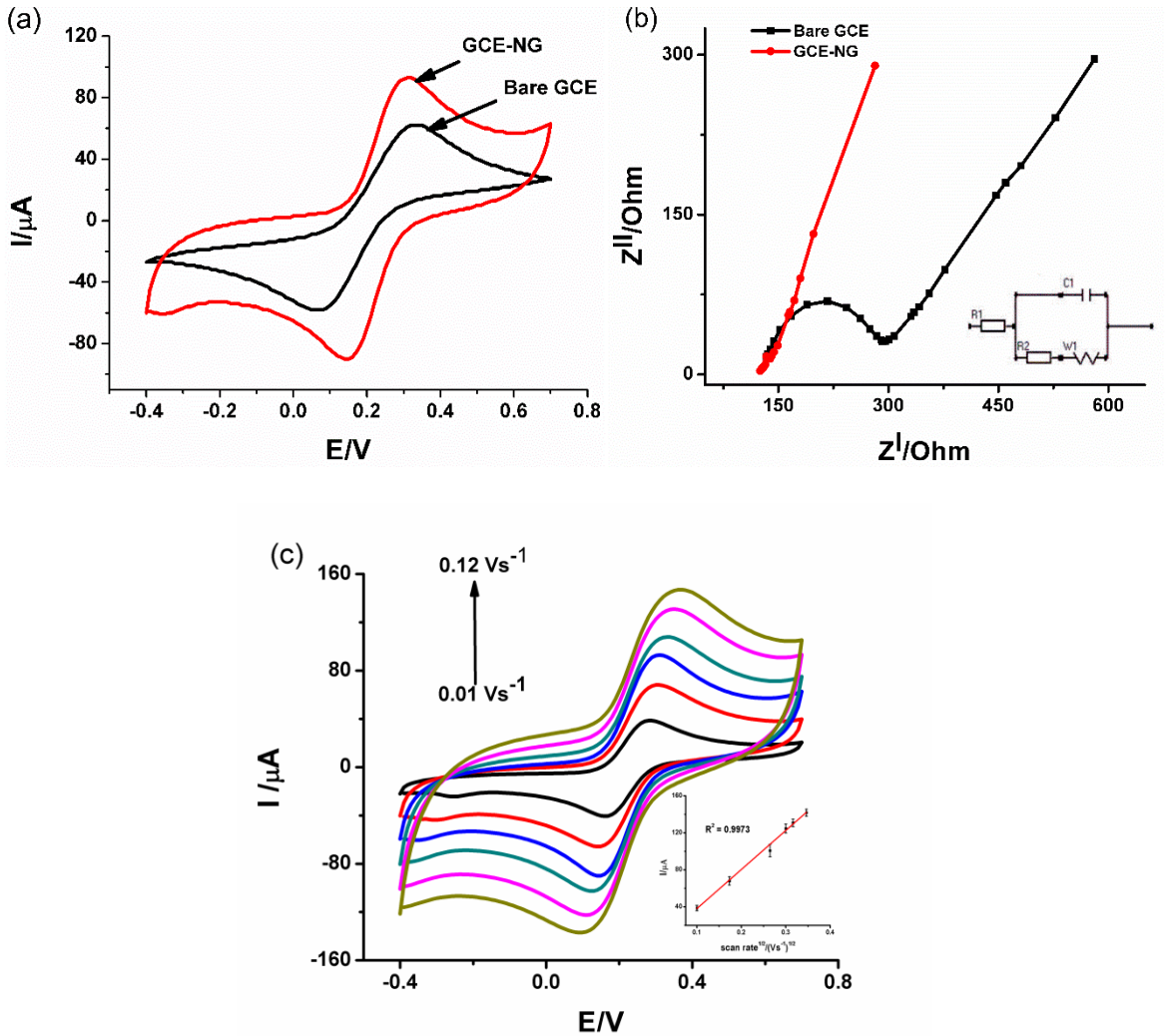

Figure 4. Electrochemical response of bare GCE and GCE-in 5 mM $[Fe(CN)_6]^{3-/4-}$ in 0.1 M KCl as supporting electrolyte, **a)** CV; **b)** Nyquist plot: Inset: Equivalent circuit employed when fitting EIS spectra and **c)** CV at different scan rates with plot of I_{pa} vs $v^{1/2}$.

The change in resistance of the modified electrode was consistent with the CV results. According to the Nyquist plot presented in **Fig. 4b**, the charge transfer resistance (R2) was 293 Ω and 123 Ω for GCE and GCE-NG, respectively. This decrease in R2 connotes a successful modification as well as the excellent electrical conductivity of NG. The electro-effective surface area of the unmodified GCE and GCE-NG were estimated from scan rate study and the gradient of the I_p vs $v^{1/2}$graph, as indicated in **Fig. 4c and 4c inset**, in a ferri/ferrocyanide solution following Randles-Sevcik **Equation 2** [23].

$$I_p = 2.69 \times 10^5 A D^{1/2} n^{3/2} C v^{1/2} \qquad \textbf{Equation (2)}$$

Where I_P = the anodic peak current (A), A = electroactive area (cm^2), D = diffusion coefficient of ferri/ferrocyanide solution, $6.1 \times 10^{-6} cm^2 s^{-1}$, n = number of electrons transferred in the redox reaction, *v* = scan rate and C = concentration of ferri/ferrocyanide ($molcm^{-3}$). The electroactive surface area for the GCE-NG (0.030871 cm^2) was about 3 times higher than that of the unmodified GCE (0.01085 cm^2). The results illustrated that the presence of NG is vital for the improved electrochemical performance of GCE-NG as it increased its electroactive surface area. Furthermore, the same plot of I_p vs $v^{1/2}$ displayed linearity (R^2 = 0.9973) which confirmed a diffusion-controlled electron transfer process on the electrode surface [24].

3.3 Optimization of parameters

3.3.1. Deposition potential

The chosen supporting electrolyte was 0.1 M $HClO_4$ at pH 1.2 [1,24,25]. A solution of 30 ppb Se(IV) in 0.1 M $HClO_4$ was used to study the effect of deposition potential during stripping as displayed in **Fig. 5a**. The potential window was set at -0.2 V to 1.2 V and preconcentration time was fixed at 25 s.

The potential scans were recorded from a negative to a positive potential (as shown by the arrow). All measurements were carried out thrice (n=3) with a percentage relative standard deviation (% RSD) less than 5%. The maximum peak current was observed at -0.8 V. Thereafter it decreased steeply due to the increasingly competitive H_2 production brought about by the hydrogen evolution reaction occurring on the electrode surface at more negative potentials [25,26]. Hence, -0.8 V was adopted as the optimal potential.

3.3.2 Deposition time

The standard solution of 30 ppb Se(IV) in 0.1 M $HClO_4$ was also used for this study, at the same potential window, with the deposition potential fixed at -0.8 V. The measurements were carried out thrice (n = 3) with % RSD less than 5%. The relationship between peak current and deposition time using the GCE-NG electrode was demonstrated in **Fig. 5b**. The peak current increased from 25s reaching its maximum at 50s. The graph exhibited a steep decrease after 100s which could be attributed to the saturation of the analyte on the electrode surface. Therefore, 50s was adopted as the optimal deposition time for this work.

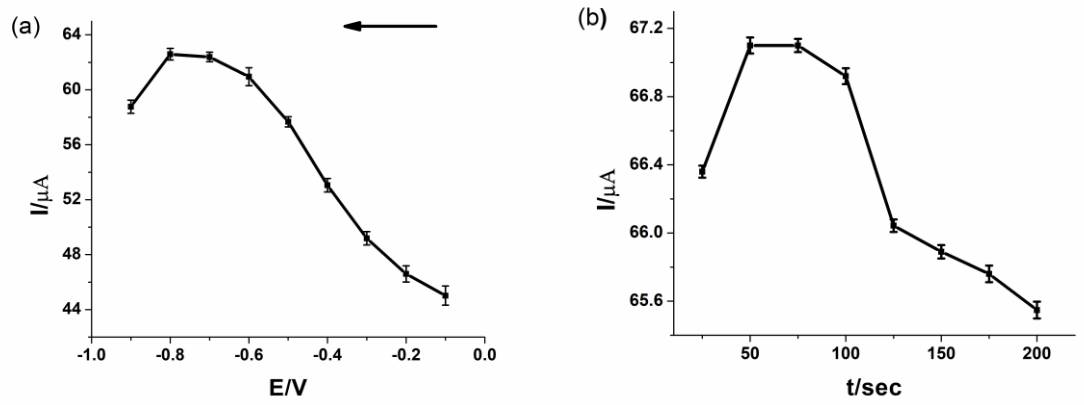

Figure 5. The effect of **a)** deposition potential and the **b)** preconcentration time on peak current during the detection of 30ppb Se(IV) in 0.1 M $HClO_4$

3.3.3 Electrochemical Detection of Selenium (IV)

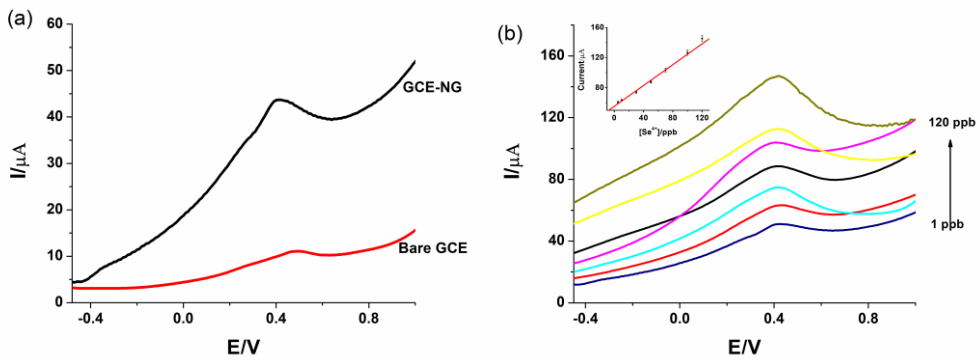

Figure 6. (a) Comparison of the performance of the unmodified GCE and GCE-NG during the detection of 30 ppb Se(IV). **(b)** GCE-NG current responses of different Se(IV) concentrations, the insert showed a calibration curve between anodic peak current and Se(IV) concentrations (n = 3).

The optimized conditions were used to determine the analytical performance of the sensor against the unmodified GCE. The unmodified GCE exhibited a lower electrochemical response in 30 ppb Se(IV) detection as indicated in **Fig. 6a.** A calibration curve as constructed using the developed sensor at concentrations ranging from 1 to 120 ppb Se(IV) (**Fig. 6b**) and the relationship between concentration and peak current showed linearity as obtained using the equation: I(μA) = 0.6915c(ppb) + 55.2447 with R^2= 0.9943. The limit of detection was calculated using the equation LOD = 3s/m, where s is the standard deviation of three SWASV measurements of the blank and m is the slope of the calibration graph. The LOD was calculated to be 0.092 ppb, which is far below the permissible level of 10 ppb. The limit of quantification (LOQ) was calculated to be 3.07 ppb. The low LOD and LOQ were attributed to the increased surface area and electrochemical conductivity resulting from modification of the bare electrode using NG. Since all the electrochemical measurements were carried out in triplicate with % RSD less than 5 %, it showed that the electrode was stable. **Table 2** presents the comparison of different

electroanalytical methods for the sensing of Se(IV) as reported in the literature. The advantage of the proposed sensor is the ease of fabrication as well as a wider linear range of concentration.

Table 2. Comparison of GCE-NG to other electrochemical sensors in literature for the determination of selenium in water.

Electrode type	Mode	Linear range (ppb)	LOD (ppb)	Matrix	Ref
AuUME	SWASV	0 -100	0.42	Tap water	[5]
GC/AuNPs/C	SWASV	5 - 55	0.175	Sea water	[26]
GC/AuNPs/E	SWASV	10-50	0.120	Sea water	[26]
Graphite SPEs	SWASV	10-1000	4.9	Tap water	[1]
GCE-AuNPs	SWASV	0.1-120	0.22	Tap water	[8]
rGO-GCE	SWASV	10-50000	0.85	Tap water	[9]
GCE-NG	SWASV	1-120	0.92	Tap water	**This work**

AuUME: Gold ultramicroelectrode; GC/AuNPS/C: Glassy carbon-gold-nanoparticles/chemically modified); GC-AuNPs/E: Glassy carbon gold nanoparticles/electrochemically modified; SPEs: screen printed electrodes.

3.4. Interference study and real water sample analysis

The presence of cations such as Cu^{2+} and Cd^{2+} have been documented to interfere when they are present with selenium in the same solution [3,8,9]. In this study standard solutions of 100 ppb, Se^{4+} containing Cd^{2+} and/or Cu^{2+} in the same concentration level were prepared. As indicated in **Fig. 7**, Cu^{2+}interfered negatively with Se^{4+} and this can be attributed to the probable preconcentration of selenium as copper selenide (Cu_2Se, Cu_3Se or CuSe) on the electrode surface [4]. Cd^{2+} also exhibited interference which was stronger when compared to Cu^{2+}**.** The combined effect Cu^{2+} and Cd^{2+} had a more pronounced negative interference on the detection Se(IV). In another study, ammonia was used as masking ligand to curb the interference of Cu^{2+} during the electrochemical sensing of As^{3+} [28]. Other approaches included the use of EDTA as a complexing agent, which reduced metal ion interferences and hence helps in improving the detection limit [4]. In this study, the addition of 0.1 M EDTA eliminated the interference of Cu^{2+} and Cd^{2+}as displayed in **Fig. 7**. This is because the presence of EDTA is reported to form bulky complexes with $Cu^{2+}$and Cd^{2+} that cannot be detected on the NG film [29].

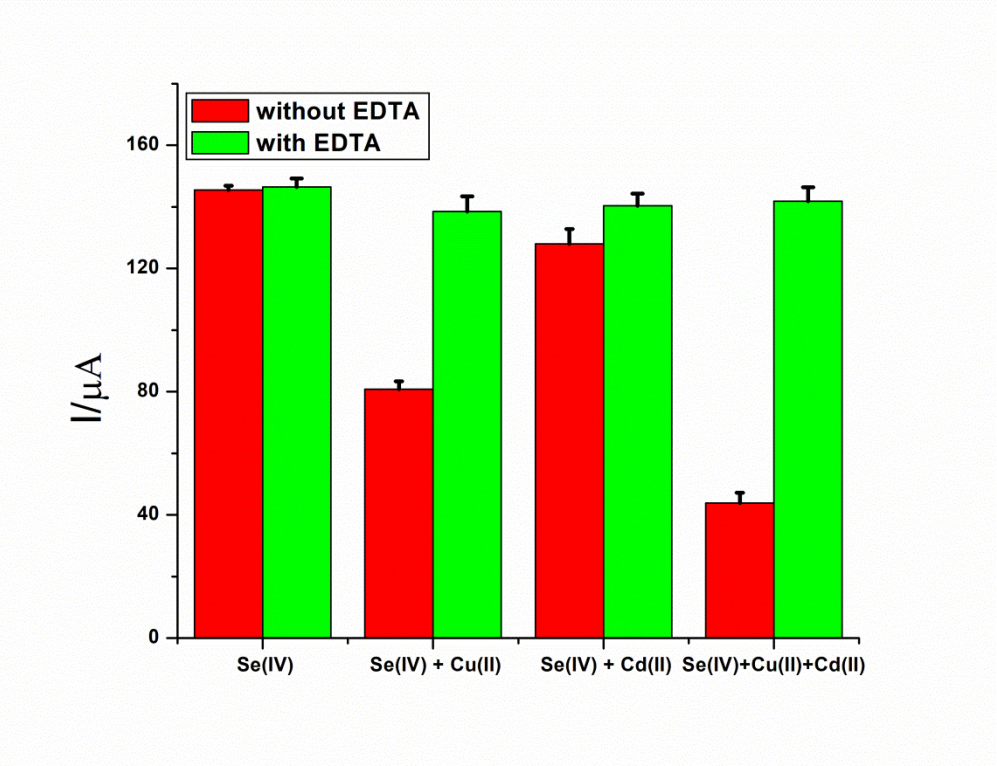

Figure 7. Interference studies under optimized experimental conditions.

To evaluate the applicability of the sensor in real water samples, the water samples were analyzed before and after spiking with a known amount of selenium ions (0.6 ppb) under the optimized conditions. The results of the GCE-NG sensor were validated by using ICP-OES as displayed in **Table 3**. Reasonable recovery percentages, which were above 95%, showed the capability of GCE-NG to determine Se(IV) in real water samples.

Table 3. Determination of Se(IV) in tap water sample *(n= 3)*

Sample	Method	Detected (ppb)	Added (ppb)	Found (ppb)	Recovery (%)
1	SWASV	0.398 ±0.0130	0.600	0.95± 0.023	95.40
1	ICP-OES	0.422 ±0.0180	0.600	1.04±0.036	101.76

4. CONCLUSION

In this study, NG was used as a smart electrode modifier for the detection of Se(IV) in standard solutions and real water samples. FT-IR, XRD and CHNS elemental analysis confirmed the successful synthesis of NG. FESEM and HRTEM studies endorsed effective nanostructuring of the GCE using the synthesized NG. Electrochemical characterization of the GCE-NG sensor was conducted using CV and EIS which proved enhanced electron conducting properties and increased the electro-effective surface area induced by the presence of NG film on the electrode surface. The sensor was able to detect Se(IV)

with a low detection limit of 0.092 ppb under optimized SWASV conditions of -0.8 V and 50 s pre concentration potential and time, respectively. The GCE-NG was successfully employed in the analysis of real water samples in the presence of EDTA, which eliminated interfering ions and the results correlated with the ICP-OES analysis with percentage recoveries greater than 95%.

ACKNOWLEDGEMENTS
This work was supported by the National Research Foundation of South Africa (Thuthuka Grant No. 107066 and CPRR Grant number: 98887); the Centre for Nanomaterials Science Research, University of Johannesburg (UJ) South Africa; the Faculty of Science, UJ South Africa and Nanotechnology Innovation Centre DST/MINTEK, University of Johannesburg (UJ) South Africa**.**

References

1. A. V Kolliopoulos, J. P. Metters, and C. E. Banks, *Anal. Methods*, 5 (2013) 851.
2. World Health Organization, *World Heal. Organ. Geneva*, (2011)
3. M. Ashournia and A. Aliakbar, *J. Hazard. Mater.*, 174 (2010) 788.
4. P. Devi, R. Jain, A.Thakur, M. Kumar, N. K. Labhsetwar, M. Nayak and P. Kumar*, TrAC - Trends Anal. Chem.*, 95 (2017) 69.
5. S. H. Tan and S. P. Kounaves, *Electroanalysis*, 10 (1998) 364.
6. X. Lin, Z. Lu, W. Dai, B. Liu, Y. Zhang, J. Li and J. Ye, *J. Electroanal. Chem.*, 828 (2018) 41.
7. H. R. Lotfi Zadeh Zhad, Y. M. Rodríguez Torres, and R. Y. Lai, *J. Electroanal. Chem.*, 803 (2017) 89.
8. A. O. Idris, N. Mabuba and A.O. Arotiba. *Int. J. Electrochem. Sci.*, 12 (2017) 10.
9. A. O. Idris, N. Mabuba, D. Nkosi, N. Maxakato, and O. A. Arotiba, *Int. J. Environ. Anal. Chem.*, 97 (2017) 534.
10. A. Benvidi, A. Dehghani-Firouzabadi, M. Mazloum-Ardakani, B. B. F. Mirjalili, and R. Zare, *J. Electroanal. Chem.*, 736 (2015) 22.
11. E. Jimenez, C. Amieva, J. L. Barroso, A. Laura, M. Hernández, and C. V. *Recent advances in graphene research*, Intech (2016) London, UK.
12. H. Cong, P. Wang, M. Gong, and S. Yu, *Nano Energy*, 3 (2014) 55.
13. C. Lei, S. Zhang, and S. Zhao, *Int. J. Electrochem. Sci.,* 12 (2017) 4856.
14. R. Yadav and C. K. Dixit, *J. Sci. Adv. Mater. Devices*, 2 (2017) 141.
15. Y. Wang, Y. Shao, D. W. Matson, J. Li, and Y. *ACS Nano*, 4 (2010) 1790.
16. M. Chen, X. Ma, and X. Li, *J. Solid State Electrochem.*, 16 (2012) 3261.
17. M. Kaur, M. Kaur, and V. K. Sharma, *Adv. Colloid Interface Sci.*, 259 (2018) 44.
18. L. Liu, *Int. J. Electrochem. Sci.*, 12 (2017) 8280.
19. T. Ida, A.*Crystal Structure Analysis,* (2013).Nagoya Institute of Technology, Japan.
20. J. Borowiec, R. Wang, L. Zhu, and J. Zhang, *Electrochim. Acta*, 99 (2013)138.
21. T. Peng, H. Sun, T. Peng, B. Liu, and X. Zhao, *Nanomaterials*, 7 (2017) 292.
22. P. Chamoli, M. K. Das, and K. K. Kar, *Curr. Graphene Sci.*, 1 (2017) 58.
23. D. Harvey, *Anal. Chem., 2 (1996)* 667
24. A. Mohammadian, M. Ebrahimi, and H. Karimi-maleh, *J. Mol. Liq.*, 265 (2018) 727.
25. E. Majid, S. Hrapovic, Y. Liu, K. B. Male, and J. H. T. Luong, *Anal. Chem*. 78 (2006) 762.
26. R. Segura, *J. Pizarroa, K. Díaza, A. Placencioa, F. Godoya, E. Pinob and F. Recio*, *Sensors Actuators, B Chem.*, 220 (2015) 263.
27. Y. Lu, X. Liang, C. Niyungeko, J. Zhou, J. Xu, and G. Tian, *Talanta*, 178 (2018) 324.
28. A. O. Idris, J. P. Mafa, N. Mabuba, and O. A. Arotiba, *Electrochem. commun.*, 64 (2016) 18.

29. J. Huang and H. Chen, *Talanta*, 116 (2013) 852.

© 2019 The Authors. Published by ESG (www.electrochemsci.org). This article is an open access article distributed under the terms and conditions of the Creative Commons Attribution license (http://creativecommons.org/licenses/by/4.0/).